Asian Journal of Chemistry; Vol. 36, No. 5 (2024), 1142-1150

ASIAN JOURNAL OF CHEMISTRY

https://doi.org/10.14233/ajchem.2024.31400

Novel Phenothiazine and Coumarin based Sensitizers: Design, Synthesis and Photoelectrochemical Application by Anchoring on CdS Nanowires

SURESH F. MADAR[1], AVINASH C. MENDHE[2], AHMEDRAZA MAVAZZAN[1], PRAVEEN K. BAYANNAVAR[1], BABASAHEB R. SANKAPAL[2], VISHWA B. NADONI[1], RAVINDRA R. KAMBLE[1,*] and MUSSUVIR PASHA[3]

[1]Department of Studies in Chemistry, Karnatak University Dharwad-580003, India
[2]Department of Physics, Visvesvaraya National Institute of Technology, Nagpur-440010, India
[3]Department of Chemistry, Karnatak Science College, Dharwad-580003, India

*Corresponding author: E-mail: ravichem@kud.ac.in

Received: 14 February 2024; *Accepted*: 30 March 2024; *Published online*: 30 April 2024; AJC-21621

Novel metal-free organic dyes (*E*)-2-cyano-3-(10-(prop-2-yn-1-yl)-10*H*-phenothiazin-3-yl)acrylic acid (PPC) and (*E*)-2-cyano-3-(10-((1-((7-methyl-2-oxo-2*H*-chromen-4-yl)methyl)-1*H*-1,2,3-triazol-4-yl)methyl)-4a,10a-dihydro-10*H*-phenothiazin-3-yl)acrylic acid (PCTC) was synthesized and then anchored to 1D cadmium sulfide nanowires (1D CdS NWs) for application in photoelectrochemical dye-sensitized solar cell (DSSC). The 1D CdS nanowires were interconnected into a nanonetwork using solution chemistry in a straightforward and efficient manner. The UV-visible spectroscopy, cyclic voltammetry and density functional theory (DFT) were effectively employed to analyze the characteristics of PPC and PCTC. The sensitizer-anchored CdS nanowires have a broader range of light absorption in the UV-visible spectrum compared to bare CdS nanowires. The complete device has the assembly FTO, compact CdS, CdS nanowires, synthesized dye and counter electrode. In photovoltaic assessment, the PCTC and PPC devices yield 3.19 and 3.04 times, respectively, more efficiency than naked CdS nanowires under conventional sunshine illumination (100 mW/cm^2, AM 1.5G). The obtained results provide strong evidence supporting the presence of rising external quantum efficiency (EQE) and show a high level of consistency with the optical tests.

Keywords: Dye-sensitized solar cells, CdS nanowires, CdS compact, Cyanoacetic acid, Sensitizers.

INTRODUCTION

As an effective device, dye-sensitized solar cells (DSSCs) have garnered significant attention due to their exceptional efficacy in transforming sunlight into electrical energy and their affordable manufacturing methods. They have been demonstrated to be a compelling tool for achieving efficient solar energy conversion, thereby warranting extensive scientific research and experimentation [1-4]. Significant research has been done on the components of DSSCs, including the sensitizers, photoanodes, counter electrodes and redox electrolytes, to enhance the performance of photovoltaic devices [5-8]. The dye sensitizer is usually an important constituent in DSSCs, as it has a significant impact on efficiency (η) and device stability. Many researchers have discovered plenty of ruthenium complex sensitizers and metal-free organic sensitizers that convert light into energy. Researchers have been interested in metal-free dyes despite their low efficiency because of their high molar extinction coefficient, easy manufacture and ecologically friendly nature [9-12]. Also the organic photosensitizers have been identified as excellent substitutes for ruthenium complex sensitizers due to the overprice and toxicity of ruthenium metal.

The common metal-free organic dye design involves a donor bridge-acceptor (D-π-A) configuration, this allows for precise adjustment of electrochemical and optical properties [13]. Triphenylamine, carbazole, coumarin, indoline and phenothiazine moieties have been effectively used as donors in metal-free organic dyes and have also shown encouraging efficiency in DSSCs of around 10% [14-17]. Phenothiazine is a heterocyclic compound that makes its analogues suitable for hole transport substances for organic devices due to its electron rich nitrogen and sulfur heteroatoms and strong capacity to give electrons. As a result, the development of inexpensive phenothiazine based sensitizers may improve the device performance

of DSSCs by changing the molecules' chemical structure.

Many low band gap and wider band gap materials have been explored with the aid of simple and low cost chemical methods [18,19] for wide spread applications like energy conversion [20], storage [21,22] and gap sensors [23]. Furthermore, chemical methods have advantages for growing nanoparticles, nanowires [24,25], *etc.* In this direction, 1D nanowires have sparked tremendous interest in production of solar cells [26], which provide direct and effective paths for charge transport, decreased electron hopping and increased interfacial area. Regarding this, our team is researching CdS nanowires photoanodes to enhance the efficacy of the photovoltaic devices by employing various novel metal-free sensitizers and altering various anchoring groups [27-29].

Current studies explore the design and synthesis of phenothiazine based sensitizers (PPC and PCTC) with cyanoacrylic acid as an anchoring group, as shown in Fig. 1. Theoretical simulations using DFT methods illustrate the shape and positioning of the HOMO and LUMOs. PPC and PCTC are utilized as metal-free organic dyes on chemically synthesized large surface area 1D CdS NWs in the production of dye-sensitized solar cells and the efficiency of the device is assessed. PCTC has shown enhanced cell efficacy compared to PPC based on current density-voltage (J-V) and external quantum efficiency (EQE) parameters. This is because there is less molecular aggregation in the case of PCTC due to derivatization from the bulky coumarin azide group to the *N*-propyl group. This is the first report of cyanoacrylic acid used as an anchoring group on CdS NWs semiconductors. The results demonstrate the potential of PCTC as a promising candidate for enhancing the efficiency of dye-sensitized solar cells. The use of cyanoacrylic acid as an anchoring group opens up new possibilities for further improving the performance of these devices.

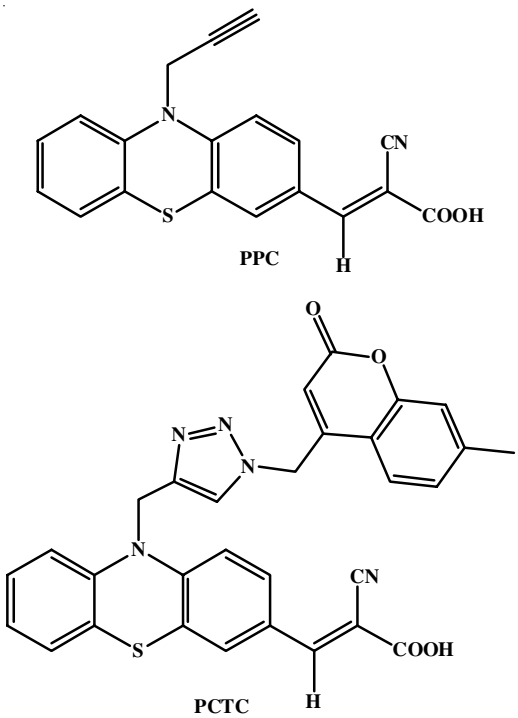

Fig. 1. Molecular structure of synthesized sensitizers PPC and PCTC

EXPERIMENTAL

Analytical-grade chemicals were utilized without purification. The reaction was monitored using thin layer chromatography on Aluchrosep silica gel 60 F_{254} plates (0.2 mm) (S.D. Fine, Mumbai, India). The melting point was obtained by using a coslab melting point equipment. The infrared spectra between 4000 and 500 cm^{-1} were recorded using Perkin-Elmer Spectrum (Version 10.5.4.). The NMR spectra were collected in response to TMS using a JEOl DELTA 2 spectrometer. A Shimadzu (LC-MS) spectrometer with a 70 eV setting was used to produce mass spectra. The elemental analyses were carried out with the help of the Heraeus CHN rapid analyzer. The Perkin-Elmer Lambda 365 UV-Vis spectrophotometer and the Jasco V-770 spectrophotometer were used to measure the UV-Vis spectra of solutions and films, respectively. A Fluoromax-4 Spectrofluorometer (Horiba) was used to record the emission spectra of solutions at ambient temperature. The substrate was a 2 mm thick fluorine doped tin oxide (FTO) coated glass with a sheet resistance of 15 /cm^2 from Sigma-Aldrich, USA.

Electrochemical measurements: The cyclic voltammetric measurements were performed in acetonitrile with a supporting electrolyte [0.10 M tetra-n-butylammonium hexafluorophosphate (TBAP)] under nitrogen environment at room temperature using a CHI-621A potentiostat workstation (scan rate: 100 mV s^{-1}). Pt wire serves as the system's counter electrode, while graphite serves as the working electrode and Ag/AgCl (saturated KCl) serves as the working electrode (reference electrode).

XRD and surface morphology measurements: A Bruker D8 advance diffractometer with Cu*K*α was used to observe X-ray diffraction in the 2θ range between 20 and 90º. Scanning electron microscopy microscopy (SEM, JEOL, SED, 5.0 KV) was used to examine the surface morphology of the films.

Photovoltaic measurements: The photocurrent-voltage properties of the DSSCs were examined using Keithly (Model: 2611A) in both light and dark environments. A Sciencetech solar simulator (Model: SS150) generated the simulated sunlight under standard conditions (100 mW/cm^2 with AM 1.5 G). EQE was calculated using a Bentham-TM 300 machine (300-800 nm) to determine how it changed with wavelength. A black painted mask was used to create an illuminated exposed area (0.20 cm^2) for each sample.

Theoretical calculations: The Gaussian 16 software was used on a computer workstation to conduct the computational studies. Utilizing the 6-311G(d,p) basis set, the hybrid B3LYP functional developed by Becke [30,31] and Lee, Yang and Parr [32] was used to optimize the ground state geometry of the organic sensitizers. For each molecule, several possible conformations were examined, and the frontier orbital computations were carried out using the conformation with the lowest energy.

Synthesis of compact CdS and CdS nanowires: Chemical bath deposition (CBD) technique was used to create a thin, compact CdS layer on FTO-coated glass by reported protocol [33]. In a nutshell, a compact layer of cadmium sulfide (CdS) was deposited to an FTO-coated glass substrate using a precursor that contained an equimolar solution of thiourea (Merck) dissolved in double distilled water and cadmium chloride (Merck),

with a maintained pH at 12 (or below) using a solution of NH_4OH (Merck). Cleansed FTO was immersed in the aforementioned precursor solution for around 40 min at 70 ºC to create a compact CdS film that was light yellow in colour.

The CBD approach was used to grow CdS NWs over a pre-coated compact CdS layer at room temperature (26 ºC), by published work [33]. An aqueous solution of 0.10 M $CdCl_2$ complexed with an aqueous ammonia solution for around 9 h was used to prepare $Cd(OH)_2$ NWs templates for CdS NWs growth, followed by the hydroxyl ions (OH^-) from the $Cd(OH)_2$ were then exchanged for S^{2-} ions in a solution of sodium sulfide flakes (Merck) for around 50 min.

Synthesis of organic sensitizers

Synthesis of 10-(prop-2-yn-1-yl)-10*H*-phenothiazine (2): Phenothiazine (3.0 g, 15.05 mmol), NaH (0.36 g, 15.05 mmol), and DMF (15 mL) were poured to a clean and oven-dried RB flask (100 mL). After stirring the reaction mixture for about 0.5 h at room temperature, propagyl bromide (2.24 mL, 15.05 mmol) was added dropwise and stirring continued overnight. Following the completion of the reaction (as indicated by TLC), the mixture was poured to clean and oven-dried beaker containing of ice-cold water (400 mL) and extracted with ethyl acetate thrice times (3 × 20 mL). Organic components were washed with brine and dried over sodium sulphate. The obtained product was purified using silica gel column chromatography and evaporated at reduced pressure to obtain a colourless viscous liquid **2** (76%).

Synthesis of 10-(prop-2-yn-1-yl)-10*H*-phenothiazine-3-carbaldehyde (3): Phosphorus oxychloride (2.76 mL, 29.50 mmol) was introduced dropwise to a round-bottom flask (100 mL) having DMF (1.15 mL, 14.75 mmol) and stirred at 0 ºC for 15 min. After stirring the aforesaid reaction mixture at room temperature for about 0.5 h, a solution of compound **2** (3.50 g, 14.75 mmol) in chloroform (10 mL) was slowly and carefully added to the reaction flask. After the addition was done, the resultant reaction mixture was heated in a water bath for 24 h until the reaction was completed (TLC). Following the completion of the reaction, the reaction mixture was cooled in ice-cold water and extracted with chloroform (3 × 20 mL). The solvent was evaporated at reduced pressure and the resultant product was purified by column chromatography by using n-hexane/ethyl acetate (7:3) as eluent. The product obtained was a yellowish-orange solid (78%).

Synthesis of 10-((1-((7-methyl-2-oxo-2*H*-chromen-4-yl)methyl)-1*H*-1,2,3-triazol-4-yl)methyl)-4a,10a-dihydro-10*H*-phenothiazine-3-carbaldehyde (4): Round bottomed flask (100 mL) was charged with 4-(azidomethyl)-2*H*-chromen-2-one (1.21 g, 5.61 mmol) obtained as reported earlier [34] and dissolved in a THF/water (1:1) mixture. Compound **3** (1.50 g, 5.61 mmol) was added to the above-prepared solution and the reaction mixture was stirred at room temperature for approximately 6 h until the reaction was completed in the presence of copper sulphate and sodium ascorbate as catalyst. After the reaction was completed (TLC), the reaction mixture was poured into ice-cold water and extracted with chloroform (3 × 20 mL). Under low pressure, the solvent evaporated and the crude product was subjected to column chromatography with an eluent mixture of *n*-hexane/ethyl acetate (7:3), yielding 2.05 g of red coloured solid of compound **4** (yield: 75%).

Synthesis of (*E*)-2-cyano-3-(10-(prop-2-yn-1-yl)-10*H*-phenothiazin-3-yl)acrylic acid (PPC): Methanol (20 mL) was added to a round-bottomed flask (100 mL) containing compound **3** (1.50 g, 5.61 mmol). Cyanoacetic acid (0.47 g, 5.61 mmol) and piperidine (0.56 mL, 5.61 mmol) were added to the above-mentioned flask and refluxed on the water bath for about 5 h until the reaction was completed. The reaction mixture was cooled to room temperature before being put into ice cold water and then acidified to neutral pH to remove excess piperidine. The resulting product was washed with distilled water followed by filtration. The dried product was purified using column chromatography with *n*-hexane/ethyl acetate (4:6) as an eluent, yielding a dark reddish solid of PPC dye (63%). IR (KBr, cm^{-1}): 3244, 2225, 2112, 1686; ^{1}H NMR (400 MHz, $CDCl_3$, δ ppm): 2.50-2.51 (1H, t, J = 4 Hz), 4.53-4.54 (2H, d, J = 4 Hz), 7.10-7.12 (1H, d), 7.20-7.28 (4H, m), 7.72-7.726 (2H, d), 7.9-7.93 (1H, dd), 8.48 (1H, s); ^{13}C NMR (100 MHz, $CDCl_3$, δ ppm): 38.5, 77.8, 79.4, 104.1, 115.5, 115.6, 116.2, 121.6, 123.0, 124.5, 127.6, 127.9, 128.5, 129.1, 130.7, 142.4, 142.6, 149.1, 162.7; MS: *m/z* ($[M]^+$): 332.07; CHN analysis for $C_{19}H_{12}N_2O_2S$ calcd. (found) %: C, 68.66 (68.65); H, 3.64 (3.65); N, 12.43 (12.44).

Synthesis of (*E*)-2-cyano-3-(10-((1-((7-methyl-2-oxo-2*H*-chromen-4-yl)methyl)-1*H*-1,2,3-triazol-4-yl)methyl)-4a,10a-dihydro-10*H*-phenothiazin-3-yl)acrylic acid (PCTC): Methanol (20 mL) was added to round-bottomed flask (100 mL) containing compound **3** (1.50 g, 5.61 mmol). Cyanoacetic acid (0.47 g, 5.61 mmol) and piperidine (0.56 mL, 5.61 mmol) were added to the above-mentioned flask and refluxed on the water bath for about 5 h until the reaction was completed. The reaction mixture was cooled to room temperature before being put into ice-cold water and then acidified to neutral pH to remove excess piperidine. The resulting product was washed with water followed by filtration. The dried product was purified using column chromatography with *n*-hexane/ethyl acetate (4:6) as an eluent, yielding a dark reddish solid of PCTC dye (62%). IR (KBr, cm^{-1}): 3428, 2962, 2932, 2219, 1724, 1690; ^{1}H NMR (400 MHz, $CDCl_3$, δ ppm): 2.37 (2H, s), 4.53 (2H, s), 5.27 (2H, s), 6.53 (1H, s), 6.93-7.10 (6H, m), 7.35-7.42 (2H, m), 7.50-7.67 (3H, m), 8.59 (1H, s); ^{13}C NMR (100 MHz, $CDCl_3$, δ ppm): 20.9, 50.0, 53.6, 105.1, 112.4, 113.9, 114.9, 115.5, 115.6, 116.2, 122.8, 123.0, 124.5, 127.5, 127.6, 127.9, 128.0, 128.5, 129.1, 130.7, 133.5, 135.4, 137.7, 138.8, 144.8, 145.1, 153.0, 155.0, 160.7, 164.1; MS: *m/z* ($[M]^+$): 547.13; CHN analysis for $C_{30}H_{21}N_5O_4S$ calcd. (found) %: C, 65.80 (65.81); H, 3.87 (3.88); N, 12.79 (12.78).

RESULTS AND DISCUSSION

Scheme-I, as illustrated, the phenothiazine was subjected to *N*-alkylation using propargyl bromide to yield 10-(prop-2-yn-1-yl)-10*H*-phenothiazine (**2**), which was then subjected to the Vilsmeir-Haack reaction to form 10-(prop-2-yn-1-yl)-4a, 10a-dihydro-10*H*-phenothiazine-3-carbaldehyde (**3**). The sensitizer PPC was prepared by combining compound **3** with cyanoacetic acid in a Knoevenagel condensation reaction. The

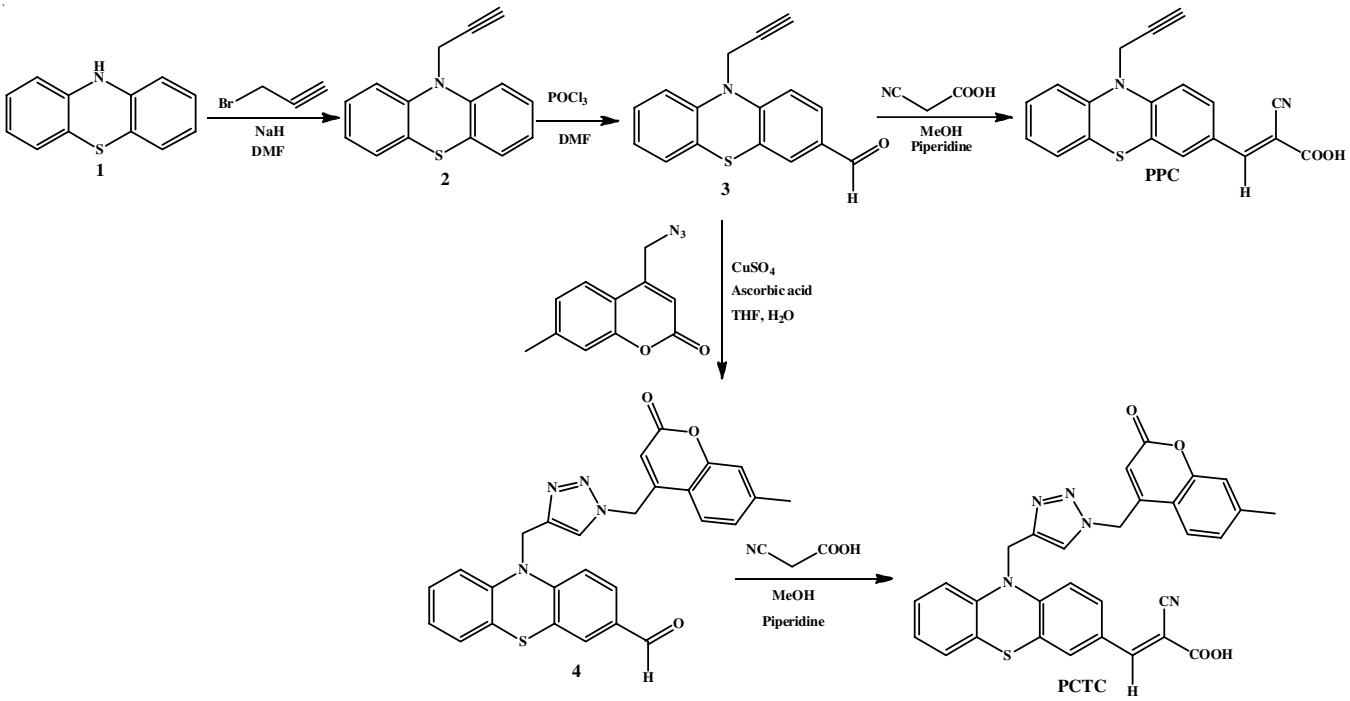

Scheme-I: Synthesis route for PPC and PCTC

PCTC was synthesized *via* click chemistry by reacting compound **3** with coumarin azide and followed by Knoevenagel condensation with cyanoacetic acid. These novel metal-free sensitizers were purified using column chromatography and then analyzed spectroscopically to validate their structure.

Structural studies: Fig. 2 displays the structure patterns in thin layer that was prepared using a standard chemical method, a mixture of FTO, CdS compact and CdS nanowires. Patterns of X-ray diffraction indicate that the deposited layers were polycrystalline. Using standard *d*-values to compare (*hkl*) planes has shown that both cubic as well as hexagonal crystal formations with spacing groups $F\bar{4}3m$ and $P\bar{6}3mc$ can work. The highest points of CdS compact thin layers were observed at

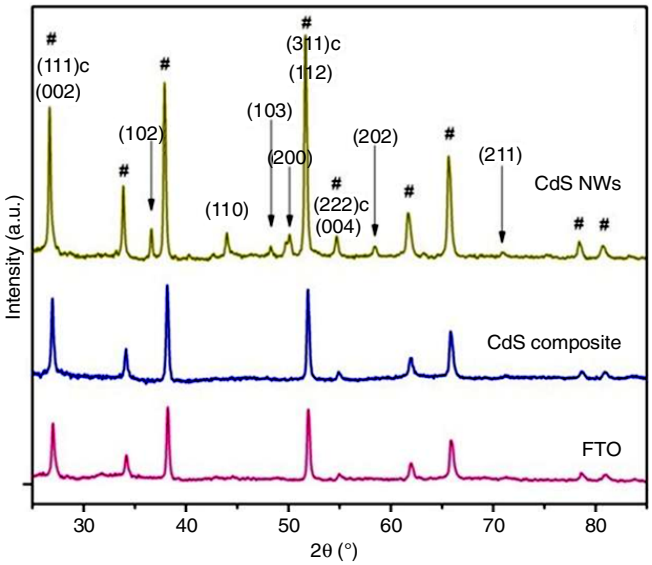

Fig. 2. X-ray diffraction patterns of FTO, CdS Compact over FTO and CdS Nanowires over FTO

crystallographic planes (111), (222) and (311). Other peaks were detected from the CdS nanowire diffraction patterns, such as (002), (102), (110), (103), (200), (112), (004), (202) and (211). The CdS compact as well as the CdS nanowires have been verified by comparing them to JCPDS cards nos. 01-080-0019 and 00-041-1049. The verification confirmed the crystal structure of CdS in the samples.

Surface characterization: Fig. 3a shows dense CdS thin layers with surfaces that resemble grains on the glass substrate covered with FTO. The extensive surface area of the CdS nanowire allows the liquid electrolyte to permeate the porous area and make direct interaction with FTO. The compact CdS layer prevents direct interaction between the liquid I_3^-/I^- and FTO. Once the ideal deposition conditions are reached, the compact surface structure serves as additional sites for the creation of CdS nanowires. Fig. 3b exhibits a nano-network within CdS at greater magnification. At greater magnification, the distinct and well-interconnected shape of the nanowires is plainly visible due to their large surface area. For enhanced device efficacy, the consistently interlinked CdS nanowires create a singular, unobstructed system for charge carriers to move through.

Optical properties: To explore the optical properties, UV-vis absorbance spectra were investigated. Fig. 4a-b show the differences in the PPC and PCTC absorbance spectra in chloroform, organic dye-loaded CdS nanowires and bare CdS nanowires. The figure depicts normalized absorbance (blue curve) with emission spectra (green curve) of PPC and PCTC dye. The spectra of both the sensitizers show two major absorbances, one in the UV region and the other in the visible region. The π-π* transition is responsible for the peaks observed at 320 nm for PPC and 335 nm for PCTC. The peaks of lower energy at 439 nm for PPC and 443 nm for PCTC result from intramolecular charge transfer (ICT) between donor and acceptor

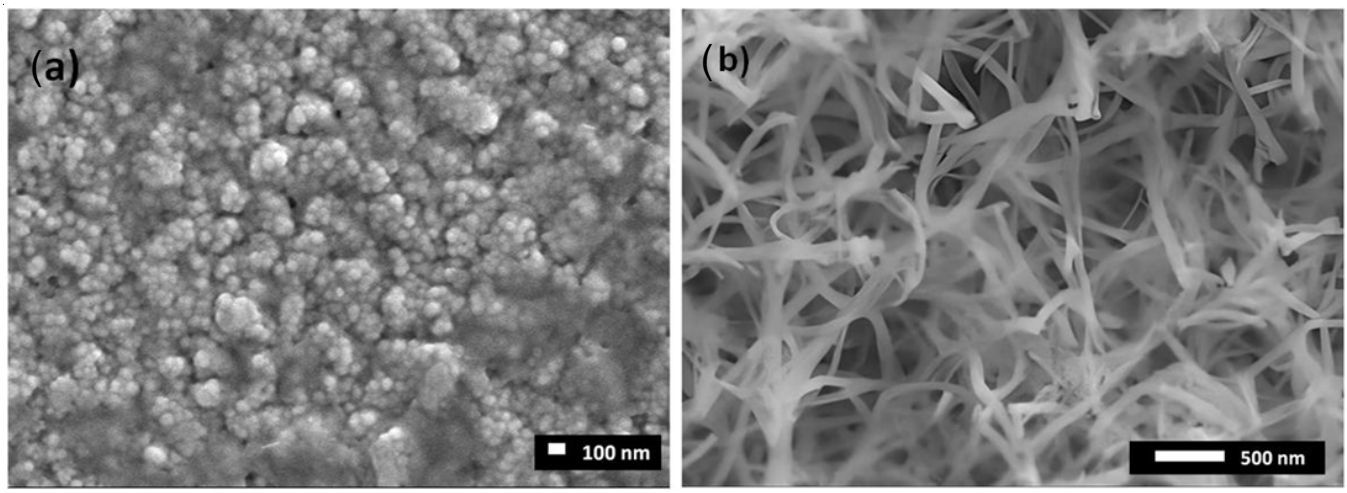

Fig. 3. Scanning electron microscope photos of (a) CdS compact (b) CdS nanowires

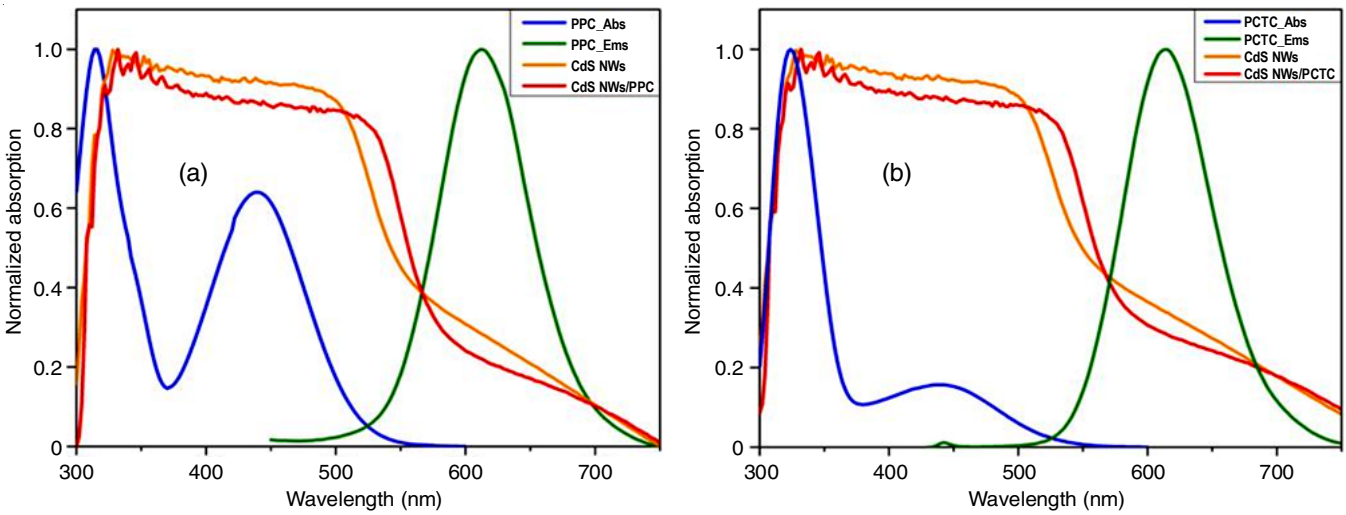

Fig. 4. Optical spectra for (a) PPC and (b) PCTC

groups, because donor and acceptor pieces undergo orbital mixing. The yellow curves in Fig. 4a-b show the absorption curve for naked CdS NWs with a shoulder around a λ_{max} of 480 nm and an onset wavelength of 506 nm indicating an energy gap of 2.42 eV. These findings corresponded to the observed band gap of CdS nanowires [35]. In addition, the absorption response of the two sensitizers attached to CdS NWs was seen as red curve. The absorption responses of the dye-CdS NWs are red-shifted and widened in comparison with the spectra of the sensitizers in chloroform and bare CdS nanowires, suggesting the existence of J-aggregation for the sensitizers with the CdS nanowires surface.

Electrochemical investigation: The electrochemical analysis of PPC and PCTC dyes were examined utilizing CV at a scan rate of 100 mV s^{-1} in an electrolyte of 0.10 M TBAP at ambient temperature in a nitrogen environment. Ferrocene was employed as a standard reference. Fig. 5 shows the CV curves of PPC and PCTC dyes in acetonitrile. It is found that HOMO-LUMO levels and electrochemical band gap by using the onset oxidation and reduction potential values along with the equations from [36]. Table-1 provides a summary of their results about HOMO-LUMO and the electrochemical band gap.

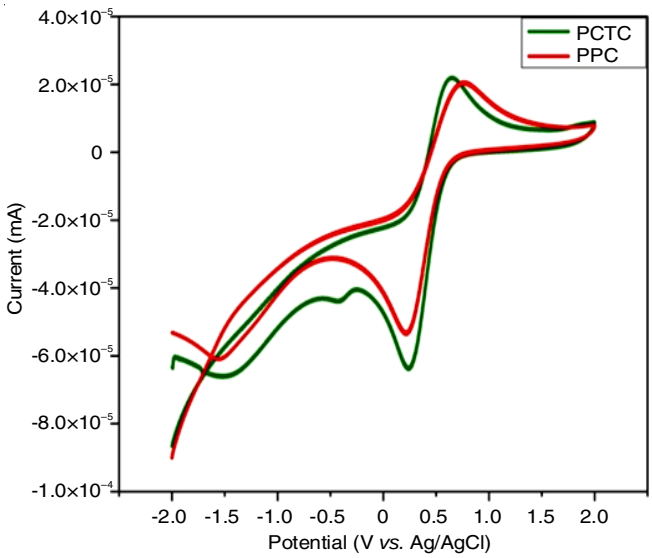

Fig. 5. CV of PPC and PCTC in 0.1 M TBAP in CH_3CN

$$HOMO = -[E^{ox}_{onset} + 0.44](eV)$$
$$LUMO = -[HOMO + E_{opt}](eV)$$
$$E^{ec}_{g} = LUMO - HOMO$$

TABLE-1
OPTICAL AND ELECTROCHEMICAL CHARACTERISTICS OF PPC AND PCTC

Label	λ_{max} (nm)[a]	λ_{max} (nm)[b]	E^{ox}_{onset} (eV)[c]	HOMO[d]	LUMO[d]	E^{ec}_{g} (eV)[d]	HOMO[e]	LUMO[e]	E_g^{DFT} (eV)[e]
PPC	439	504	0.64	-5.08	-2.26	2.82	-5.87	-3.00	2.87
PCTC	443	506	0.71	-5.15	-2.35	2.80	-5.94	-2.87	3.07

[a]Absorptions in $CHCl_3$ solution; [b]Absorptions on a CdS nanowires; [c]Oxidation potential relatives to Ag/AgCl electrode; [d]HOMO, LUMO energy levels and optical band gap (CV method); [e]HOMO, LUMO energy levels and Optical band gap (DFT method).

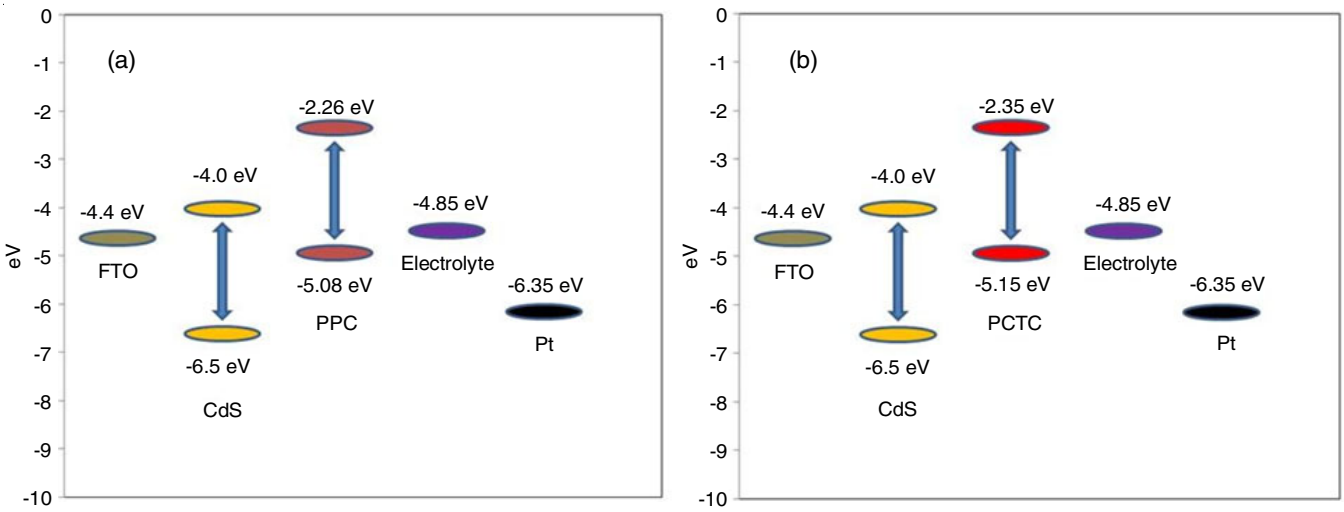

Fig. 6. A schematic energy band diagram for fabricated device with sensitizers (a) PPC and (b)PCTC

The CdS nanowires have a conduction band energy of -4.0 eV, while the LUMO of PPC and PCTC were -2.26 eV and -2.35 eV, respectively. It indicates that transferring excited electrons from organic dyes to conduction band of semiconductors (CdS NWs) is thermodynamically favourable. The HOMO of PPC and PCTC was -5.08 eV and -5.15 eV, respectively, both smaller than the -4.8 eV value of the I_3^-/I^- redox pair. This makes sure that the oxidized sensitizers produced when an electron is introduced into the CdS NWs conduction band can effectively receive an electron by the I^- of the I_3^-/I^- pair. PPC has an energy band gap of 2.82 eV, while PCTC has a band gap of 2.80 eV. Fig. 6 shows the energy level diagram for devices made with PPC and PCTC sensitizers. The energy band diagram shows that the highest occupied molecular orbital (HOMO) levels of PPC and PCTC matched well with the conduction band of CdS nanowires, which makes it easier for electrons to move through them. The results suggest that devices utilizing these dyes could exhibit enhanced efficiency in dye-sensitized solar cells.

Computational studies: The shapes and electronic arrangement of the organic dyes (PPC and PCTC) were determined using density functional theory (DFT) calculations at the B3LYP/6-31G(d) level.

Molecular electrostatic potential maps (MEP): Fig. 7 illustrates the electrostatic potential of organic dyes (PPC and PCTC) using a rainbow colour pattern. The deepest red hue signifies an electron-rich location that could be attractive to electrophiles. The electron-deficient region with a blue hue might draw molecules towards nucleophiles. The red region in the MEP diagram of PPC molecule is situated on the carbonyl oxygen of the cyanoacrylic acid group. The colour blue serves

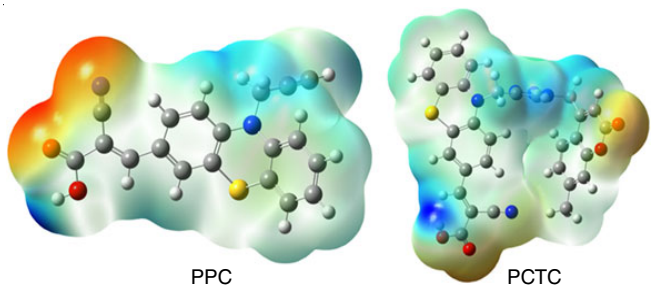

Fig. 7. MEP images of PPC and PCTC

as a visual cue for the H-atom in the carboxylic group that is devoid of electrons. The PCTC displays a prominent red colour above the carbonyl oxygens of coumarin and carboxylic acid, indicating a region abundant in electrons. The dark blue patch covers the hydrogen atom of carboxylic group, which is a location with a deficiency of electrons vulnerable to nucleophile. The MEP suggests that the acceptor group, particularly carboxylic, can bind to the semiconductor surface. This binding interaction is crucial for the molecule's adsorption properties on the surface. Understanding the MEP diagram can provide insights into the reactivity and behaviour of the PPC molecule in various applications.

Frontier molecular orbital (FMO): The HOMO energy level for the organic dyes PPC and PCTC was mostly on the phenothiazine ring and a small part of the π-linker. Frontier LUMO energy level was located on the cyanoacrylic acid group, the π-linker and a small part of the phenothiazine ring, as depicted in Fig. 8. This splits the electron transfer from the phenothiazine group (donor) to the cyanoacrylic acid group (acceptor) *via* the π-bridge, making sure that the electrons are

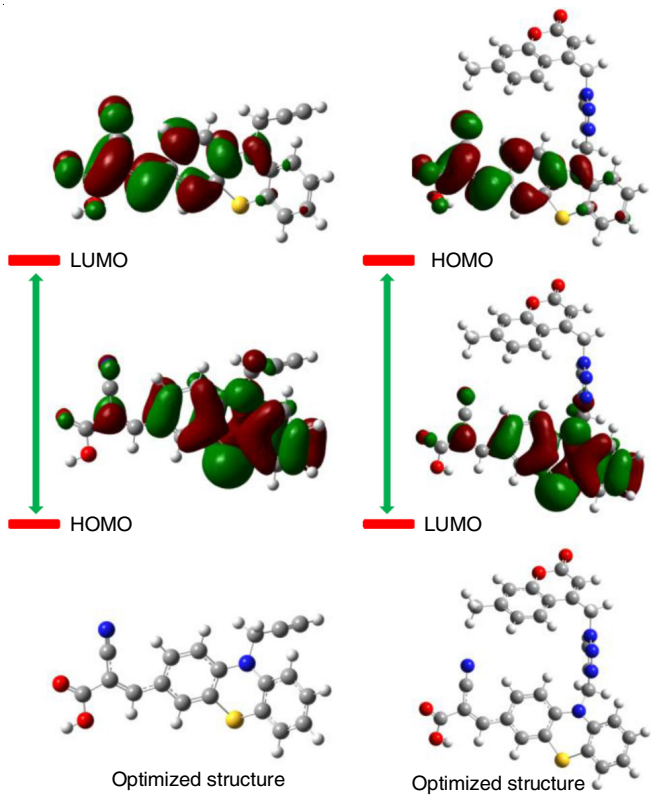

Fig. 8. HOMO-LUMO and optimized structure of (a) PCTC and (b) PPC

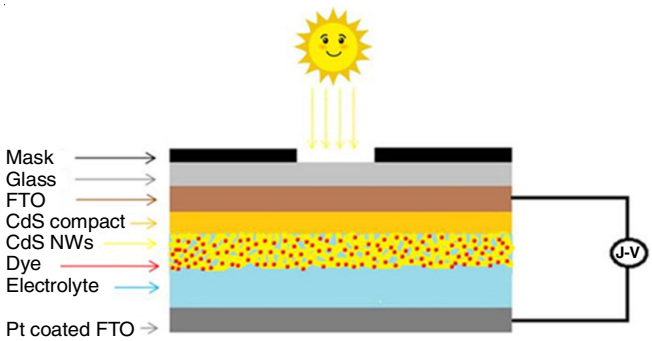

Fig. 9. A schematic illustration of the device

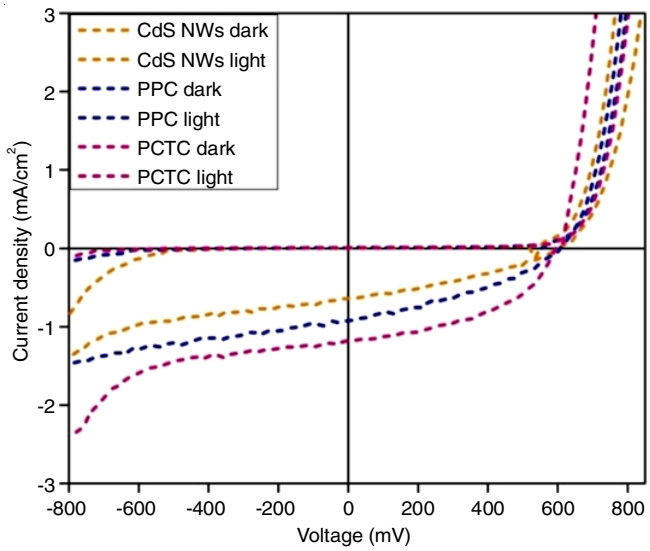

Fig. 10. J-V characterization plots

injected and charges are separated efficiently. They also make it easier for electrons to move from the excited sensitizer to the conduction band of the CdS semiconductor when the LUMOs are attached to the surface of CdS nanowires. Table-1 displays the theoretically computed HOMO, LUMO and energy band gap values of PPC and PCTC. Theoretical DFT results were compared to electrochemical values, showing good agreement. A few minor differences between both of them can be explained by the distinct molecular environments: electrochemical data was collected in the liquid state, while DFT data was collected only in a gaseous state.

Photovoltaic properties: The developed device is schematically represented in Fig. 9, which demonstrate its structure as FTO/CdS Compact/CdS nanowires/sensitizer/(I_3^-/I^-)/Pt.

The photovoltaic cell efficiencies of PPC and PCTC as dye-sensitizers were analyzed through photocurrent density against voltage (J-V) measurements. Fig. 10 displays the J-V graphs for CdS nanowires and CdS NWs loaded with dye. The J_{SC}, V_{OC} and FF of PPC and PCTC were determined and the results are shown in Table-2. The J-V measurements were conducted for the devices within the voltage span from -1.0 to +1.0 V in dark and bright illumination conditions. The naked CdS NWs exhibited an efficiency (η) of 0.102% under light. The efficiency of the sensitizer-loaded CdS NWs was 0.31% for PPC and 0.324% for PCTC. The inclusion of a larger coumarin group in PCTC reduces molecular agglomeration and demonstrates higher effectiveness than PPC, as shown in DFT simulations. Table-2 contains the assessed results of series resistance (R_s) and shunt resistance (R_{sh}) for fabricated DSSCs. The R_{sh} and R_s values for PPC and PCTC are also provided in Table-2, exhibiting differences in the performance of the PPC and PCTC loaded CdS nanowires. These values further support the higher efficiency of PCTC compared to PPC due to reduced molecular agglomeration.

External quantum efficiency (EQE): The EQE of CdS nanowires loaded with PPC and PCTC in I_3^-/I^- electrolyte was plotted against wavelength, showing response across the visible spectrum ranging from 300 to 600 nm. Fig. 11 demonstrates a noticeable change in the EQE for CdS nanowires as well as PPC and PCTC loaded CdS nanowires. The minimum EQE value found for CdS nanowires was 7.56%. The enhanced EQE values are 45.45% for PCTC loaded CdS nanowires and 44.12% for PPC loaded CdS nanowires. The results align with the J-V inves-

TABLE-2
THE PHOTOVOLTAIC OUTPUTS FOR THE DSSC

Label	J_{sc} (mA/cm^2)	V_{oc} (V)	FF (%)	η (%)	R_{sh} (kΩ)	R_s (Ω)
CdS NWs	0.568	0.544	33.0	0.102	214.16	116.24
CdS NWs/PPC	0.963	0.611	52.7	0.31	669.27	58.31
CdS NWs/PCTC	1.208	0.603	44.8	0.326	794.35	39.34

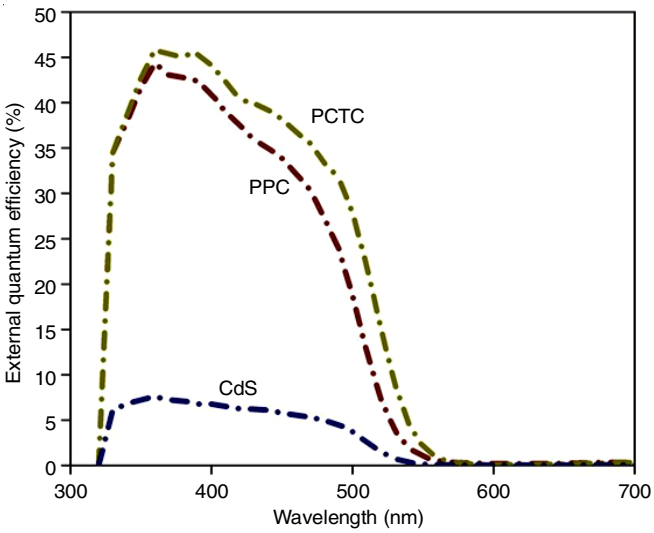

Fig. 11. External quantum efficiency spectra of the DSSCs

tigations. These findings suggest that the incorporation of PPC and PCTC significantly improves the efficiency of CdS nanowires in solar cell applications. The observed increase in EQE values highlights the potential for enhanced performance in photovoltaic devices utilizing these materials.

Conclusion

This study focused on designing, synthesizing and testing the efficiency of two new organic dye-sensitizers, PPC and PCTC, which are derived from phenothiazine. These sensitizers were anchored on 1D-CdS nanowires for use in DSSC. Both sensitizers contain phenothiazine as the main component, acting as an electron donor group and cyanoacetic acid as an anchoring group. Furthermore, PCTC consist of a coumarin ring and a triazole ring, which are linked to the phenothiazine structure by adopting the simple synthetic method. The PCTC sensitizer, with a concentration of 0.324%, exhibits higher efficiency in solar energy absorption compared to PPC (0.31%) and naked CdS nano-wires (0.102%). The DFT and the external quantum efficiency (EQE) results are highly relevant to the photovoltaic experiments. Since, both PCTC and PPC being effective sensitizers commonly employed in DSSC applications can enhance the efficiency of bare CdS NWs by factors of 3.04 and 3.19, respectively.

ACKNOWLEDGEMENTS

One of the authors, SFM, expresses his gratitude towards CSIR, New Delhi, for granting the JRF. The authors express gratitude to DST-PURSE Phase-II, DST-SAIF, the USIC, Karnatak University, Dharwad and the University of Mysore, Mysuru, India, for supplying the UPLC mass spectral data and research facility. The authors express gratitude to VNIT, Nagpur, India for facilitating the solar simulation investigations.

CONFLICT OF INTEREST

The authors declare that there is no conflict of interests regarding the publication of this article.

REFERENCES

1. B. O'Regan and M. Graetzel, *Nature*, **353**, 737 (1991); https://doi.org/10.1038/353737a0
2. W.Q. Wu, H.L. Feng, H.S. Rao, Y.F. Xu, D.B. Kuang and C.Y. Su, *Nat. Commun.*, **5**, 3968 (2014); https://doi.org/10.1038/ncomms4968
3. W.Q. Wu, Y.F. Xu, H.S. Rao, C.Y. Su and D.B. Kuang, *J. Am. Chem. Soc.*, **136**, 6437 (2014); https://doi.org/10.1021/ja5015635
4. W.Q. Wu, Y.F. Xu, H.S. Rao, H.L. Feng, C.Y. Su and D.B. Kuang, *Angew. Chem. Int. Ed.*, **53**, 4816 (2014); https://doi.org/10.1002/anie.201402371
5. J.S. Ni, J.H. You, W.I. Hung, W.S. Kao, H.H. Chou and J.T. Lin, *ACS Appl. Mater. Interfaces*, **6**, 22612 (2014); https://doi.org/10.1021/am5067145
6. A. Mishra, M.K.R. Fischer and P. Bäuerle, *Angew. Chem. Int. Ed.*, **48**, 2474 (2009); https://doi.org/10.1002/anie.200804709
7. J. Dong, J. Wu, J. Jia, L. Fan and J. Lin, *J. Colloid Interface Sci.*, **498**, 217 (2017); https://doi.org/10.1016/j.jcis.2017.03.025
8. D. Barpuzary, A.S. Patra, J.V. Vaghasiya, B.G. Solanki, S.S. Soni and M. Qureshi, *ACS Appl. Mater. Interfaces*, **6**, 12629 (2014); https://doi.org/10.1021/am5026193
9. S.L. Li, K.J. Jiang, K.F. Shao and L.M. Yang, *Chem. Commun.*, 2792 (2006); https://doi.org/10.1039/b603706b
10. N. Koumura, Z.S. Wang, S. Mori, M. Miyashita, E. Suzuki and K. Hara, *J. Am. Chem. Soc.*, **128**, 14256 (2006); https://doi.org/10.1021/ja0645640
11. T. Horiuchi, H. Miura, K. Sumioka and S. Uchida, *J. Am. Chem. Soc.*, **126**, 12218 (2004); https://doi.org/10.1021/ja0488277
12. S. Ramkumar and S. Anandan, *Dyes Pigments*, **97**, 397 (2013); https://doi.org/10.1016/j.dyepig.2013.01.014
13. A.S. Hart, C.B. K. C, N.K. Subbaiyan, P.A. Karr and F. D'Souza, *ACS Appl. Mater. Interfaces*, **4**, 5813 (2012); https://doi.org/10.1021/am3014407
14. S. Ito, H. Miura, S. Uchida, M. Takata, K. Sumioka, P. Liska, P. Comte, P. Péchy and M. Grätzel, *Chem. Commun.*, 5194 (2008); https://doi.org/10.1039/b809093a
15. P.Y. Ho, C.H. Siu, W.H. Yu, P. Zhou, T. Chen, C.L. Ho, L.T.L. Lee, Y.H. Feng, J. Liu, K. Han, Y.H. Lo and W.Y. Wong, *J. Mater. Chem. C Mater. Opt. Electron. Devices*, **4**, 713 (2016); https://doi.org/10.1039/C5TC03308J
16. A. Sen and A. Groß, *ACS Appl. Energy Mater.*, **2**, 6341 (2019); https://doi.org/10.1021/acsaem.9b00973
17. W. Xu, B. Peng, J. Chen, M. Liang and F. Cai, *J. Phys. Chem. C*, **112**, 874 (2008); https://doi.org/10.1021/jp076992d
18. P.R. Nikam, P.K. Baviskar, J.V. Sali, K.V. Gurav, J.H. Kim and B.R. Sankapal, *Ceram. Int.*, **41**, 10394 (2015); https://doi.org/10.1016/j.ceramint.2015.03.239
19. R.S. Mane, B.R. Sankapal and C.D. Lokhande, *Thin Solid Films*, **359**, 136 (2000); https://doi.org/10.1016/S0040-6090(99)00532-5
20. D.B. Salunkhe, S.S. Gargote, D.P. Dubal, W.B. Kim and B.R. Sankapal, *Chem. Phys. Lett.*, **554**, 150 (2012); https://doi.org/10.1016/j.cplett.2012.10.032
21. S.A. Pande, B. Pandit and B.R. Sankapal, *Mater. Lett.*, **209**, 97 (2017); https://doi.org/10.1016/j.matlet.2017.07.084
22. B. Pandit, G.K. Sharma and B.R. Sankapal, *J. Colloid Interface Sci.*, **505**, 1011 (2017); https://doi.org/10.1016/j.jcis.2017.06.092
23. N.B. Sonawane, K.V. Gurav, R.R. Ahire, J.H. Kim and B.R. Sankapal, *Sens. Actuators A Phys.*, **216**, 78 (2014); https://doi.org/10.1016/j.sna.2014.05.012
24. A.C. Mendhe, S. Majumder, N. Nair and B.R. Sankapal, *J. Colloid Interface Sci.*, **587**, 517 (2021); https://doi.org/10.1016/j.jcis.2020.11.031

25. P.K. Bayannavar, A.C. Mendhe, B.R. Sankapal, M.S. Sannaikar, S.K. J. Shaikh, S.R. Inamdar and R.R. Kamble, *J. Mol. Liq.*, **336**, 116862 (2021); https://doi.org/10.1016/j.molliq.2021.116862
26. Z. Zhou, J. Fan, X. Wang, W. Zhou, Z. Du and S. Wu, *ACS Appl. Mater. Interfaces*, **3**, 4349 (2011); https://doi.org/10.1021/am201001t
27. P.K. Bayannavar, A.C. Mendhe, M.S. Sannaikar, S.R. Inamdar, B.R. Sankapal, R.R. Kamble, M.Y. Kariduraganavar, S.F. Madar and A. Mavazzan, *Colloids Surf. A Physicochem. Eng. Asp.*, **640**, 128500 (2022); https://doi.org/10.1016/j.colsurfa.2022.128500
28. A. Mavazzan, R.R. Kamble, A. Mendhe, B.R. Sankapal, P.K. Bayannavar, S.F. Madar, T.V. Metre, K.M. Mussuvir Pasha, B. Kodasi and V.B. Nadoni, *Physica B*, **668**, 415253 (2023); https://doi.org/10.1016/j.physb.2023.415253
29. S.F. Madar, A.C. Mendhe, A. Mavazzan, P.K. Bayannavar, B.R. Sankapal, R.R. Kamble, V.B. Nadoni and K.M. Mussuvir Pasha, *Mater. Sci. Eng. B*, **300**, 117035 (2024); https://doi.org/10.1016/j.mseb.2023.117035
30. A.D. Becke, *J. Chem. Phys.*, **98**, 5648 (1993); https://doi.org/10.1063/1.464913
31. A.D. Becke, *Phys. Rev.*, **38**, 3098 (1988); https://doi.org/10.1103/PhysRevA.38.3098
32. C. Lee, W. Yang and R.G. Parr, *Phys. Rev. B Condens. Matter Mater. Phys.*, **37**, 785 (1988); https://doi.org/10.1103/PhysRevB.37.785
33. A.C. Mendhe, S. Majumder, S.M. Pawar and B.R. Sankapal, *Surfaces and Interfaces*, **27**, 101457 (2021); https://doi.org/10.1016/j.surfin.2021.101457
34. S.M. Somagond, R.R. Kamble, P.K. Bayannavar, S.K.J. Shaikh, S.D. Joshi, V.M. Kumbar, A.R. Nesaragi and M.Y. Kariduraganavar, *Arch. Pharm. Chem. Life Sci.*, **10**, 352 (2019); https://doi.org/10.1002/ardp.201900013
35. A.C. Mendhe, P. Babar, P. Koinkar and B.R. Sankapal, *J. Taiwan Inst. Chem. Eng.*, **133**, 104251 (2022); https://doi.org/10.1016/j.jtice.2022.104251
36. M.N. Kumbar, M.S. Sannaikar, S.J. Shaikh, A.A. Kamble, M.N. Wari, S.R. Inamdar, Q. Qiao, B.N. Revanna, M. Madegowda, J.P. Dasappa and R.R. Kamble, *Photochem. Photobiol.*, **94**, 261 (2018); https://doi.org/10.1111/php.12852